Numerical Simulation and Analysis of a 3D Continuous Detonation under Rocket Engine Conditions

Yohann EUDE, Dmitry DAVIDENKO,* Iskender GÖKALP,* and François FALEMPIN***
**ICARE – CNRS*
1C Avenue de la Recherche Scientifique, 45071 Orléans, France
***MBDA France*
1 Avenue Réaumur, 92358 Le Plessis Robinson, France

Abstract
The paper presents the computational method and results of 2D and 3D numerical simulations of the flowfield under conditions of a Continuous Detonation Wave Rocket Engine (CDWRE). Numerical simulations have been performed using a detailed thermochemical model of H_2-O_2 mixture and a high-resolution Euler code with the Adaptive Mesh Refinement (AMR) method. Main features of 2D and 3D flowfields are described. Conditions of detonation propagation in a layer of fresh mixture are analyzed. It is shown that the detonation propagates in the Chapman-Jouguet mode.

1. Introduction

During the last decade, the interest in the use of continuously propagating detonation waves in aerospace propulsors has been quickly growing. Both experimental and computational studies are under way in different countries. In France, ICARE-CNRS is closely collaborating with MBDA France and contributing to the theoretical and numerical studies on Continuous Detonation Wave Rocket Engines (CDWRE).
First numerical simulations of CDWRE chambers are known from publications by Zhdan et al. [1, 2]. These simulations were performed on a 2D periodic domain assuming uniformly distributed injection. 3D and viscous effects were neglected. A global kinetic model of stoichiometric H_2-O_2 mixture, based on an ignition delay time approximation, and the calorically perfect gas model were applied.
Following the computational approach proposed by Zhdan et al., several numerical studies have been conducted using various thermochemical models and numerical techniques. Hishida et al. [3] used a single-reaction kinetic model to simulate the continuous detonation in a H_2-air mixture with high spatial resolution that was sufficient to resolve the cellular structure of detonation and hydrodynamic instabilities on the boundary of the fresh mixture layer. Detailed kinetic models of H_2-O_2 mixture were applied by Davidenko et al. [4, 5] and Yamada et al. [6]. Davidenko et al. conducted a parametric study by varying injection and geometrical parameters of the chamber; whereas Yamada et al. tried to find limits of stable detonation propagation.
3D results are known from publications by Shao et al. [7, 8] and Yi et al. [9, 10]. These 3D simulations were performed using single-step reaction and calorically perfect gas models. More recently, 3D simulations with a detailed kinetic model of H_2-O_2 mixture were conducted by Eude et al. [11]. The obtained results provide information on the 3D flow structure and chamber performance for different injection conditions and forms of the duct.
The present work is aimed at obtaining 2D and 3D results by solving the Euler equations with the same thermochemical model and numerical methods, but for different injection configurations: uniformly distributed injection in 2D and slot injection in 3D. The adaptive mesh refinement (AMR) is applied to efficiently manage the computational mesh. 2D and 3D results are presented to demonstrate 3D effects. Detonation propagation in a layer of fresh mixture is analyzed in comparison with the theoretical Chapman-Jouguet mode.

2. Principle of CDWRE operation

According to the CDWRE concept, propellants are continuously injected in a combustion chamber that can be shaped as a radial or cylindrical duct. One or more transverse detonation waves move across the flow of combustible mixture. Due to the continuous injection, the mixture layer is restored between successive detonation waves. In the moving frame related to a detonation front, the mean flow is globally steady state.

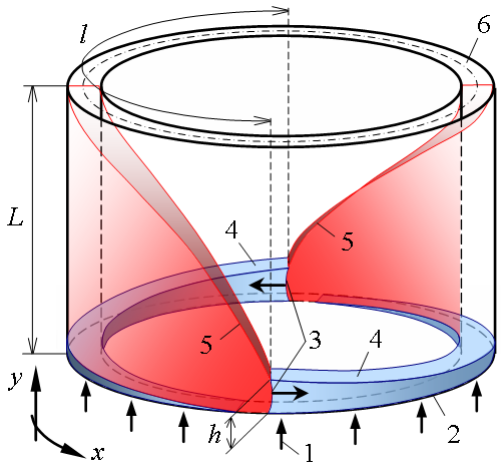

Figure 1: Schematic of a CDWRE combustion chamber

For propulsion applications, an annular cylindrical combustion chamber is the most appropriate configuration. It is schematically shown in Fig. 1. A mixture of fuel and oxidizer (1) is injected from the closed end (2) of the chamber through ring slits or regularly arranged small holes. Transverse detonation waves (3) burn the layer of combustible gas (4). The azimuthal direction of detonation propagation is defined at the initiation and does not change if the detonation is stable. The thickness of the fresh mixture layer, h, and the spatial period, l, between successive detonation fronts are proportional and depend on the propellants and injection conditions [12]. The detonation is close to the Chapman-Jouguet mode so the detonation frequency (inverse time period between successive detonations) is of the order of 10 kHz. The detonation waves induce oblique shocks (5) in the burnt gas. The combustion products flow toward the duct open end (6) and then discharge from the chamber through a divergent nozzle (not shown in the scheme). Due to the combustion product expansion, a supersonic flow velocity can be achieved though the device has no geometrical throat.

3. Computational approach

The aim of this study is to examine 3D effects due to the slot injection. Hence we make a step from the purely 2D configuration with uniformly distributed injection to a 3D one with slot injection while keeping the following features unchanged:

– periodical flow in the direction of detonation propagation;
– viscous effects are neglected both in the flow core and on the walls;
– infinitely large radius of the chamber (no curvature effects).

3.1 Problem formulation

Numerical simulation of a CDWRE combustion chamber in the full 3D configuration is quite expensive. The computational cost can be significantly reduced due to the flowfield periodicity in the direction of detonation propagation. Experimental photographic records [12, 13] show that the flow structure is repetitive with a constant spatial period. Applying azimuthal periodicity, the x-wise extent of the computational domain can be taken equal to l as illustrated in Fig. 2. In 3D, the flowfield is symmetric in the z direction. Using the symmetry property, only a half of the duct is included in the computational domain.

The 2D computational domain represents a rectangle $l \times L$. The 3D domain is composed of two parallelepipeds: the chamber duct $l \times L \times \Delta/2$ and the injection slot $l \times L_j \times \Delta_j/2$. For the case considered in the present study, the following geometrical sizes are taken: $l = 50$ mm; $L = 20$ mm; $\Delta = 5$ mm; $L_j = 0.9$ mm; $\Delta_j = 0.3$ mm.

The 2D and 3D domains have three boundaries of the same kinds: two periodic boundaries and a free outflow boundary (see Fig. 2). In 3D, symmetry or slip wall conditions are used on the boundaries representing the symmetry plane, the duct and slot walls.

The injection conditions are defined as follows: H_2-O_2 stoichiometric mixture as injectant composition; the total temperature $T_{tj} = 300$ K; and the total pressure $P_{tj} = 1$ MPa. In 2D, it is supposed that the mixture is injected through infinitely small sonic injectors, which are uniformly distributed over the injection wall. This kind of boundary is characterized by the relative injection area $A_j / A_w = 0.133$, where A_j is the net area of injector throats and A_w is the

overall area of the injection wall. In 3D, the injection area is limited by the slot width, Δ_j, that represents 6 % of the duct width, Δ.

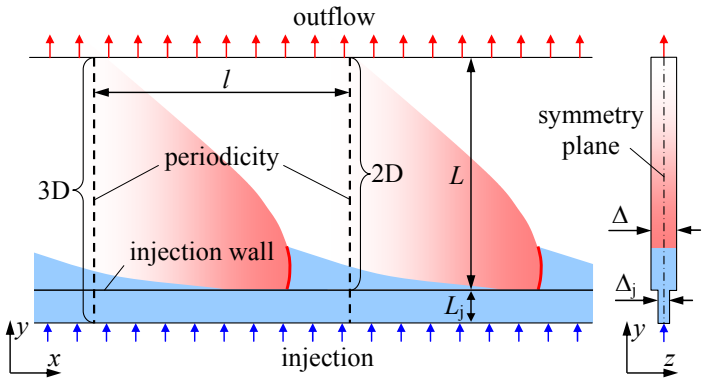

Figure 2: Schematic of periodic computational domain in 2D and 3D

For both configurations, the injection mass flow rate is locally evaluated using the following method. The flow in the injectors is assumed isentropic to establish relations between the total injection parameters and the static injection conditions. Depending on the local pressure on the injection boundary, P_w, the local injection mass flux, g_j, is allowed to vary from zero at $P_w \geq P_{tj}$ to $g_{j\,cr}$ at $P_w \leq P_{j\,cr}$, where $P_{j\,cr}$ is the pressure at which the sonic injection condition is achieved. This also implies that the gas from the chamber may not penetrate in the injectors.

3.2 Thermochemical model

A finite-rate kinetic model is adopted not only to describe combustion reactions in the detonation wave but also to simulate the non-equilibrium processes during the combustion product expansion. This model is represented by a kinetic mechanism including 6 species (H_2, O_2, H_2O, H, O, and OH) and 7 reversible chemical reactions [14]. The rate constants of the backward reactions have been refitted in a temperature range up to 4000 K suitable for detonation simulations. Standard thermodynamic properties of pure species [15] are approximated by piecewise linear functions for the species specific heats and piecewise quadratic functions for the species enthalpies. On a large number of sufficiently small temperature intervals, this kind of approximation is found to be precise and considerably less time-consuming than the standard temperature polynomials.

3.3 Numerical method

Neglecting viscous interactions, the high Reynolds number flow of reacting gas can be described by a system of Euler equations that includes transport equations for all but one chemical species. A high-resolution numerical solver, based on the finite-difference method, is used. For the numerical flux approximation, the shock-capturing, weighted essentially non-oscillatory (WENO) scheme of the fifth order [16] is employed together with the Lax-Friedrichs splitting of fluxes in the characteristic form. For the time integration, the ASIRK2C second-order semi-implicit additive Runge-Kutta scheme [17] is used. The convective terms in the governing equations are treated explicitly while the implicit treatment is applied to the source terms. The time step is controlled by the Courant-Friedrichs-Lewy stability condition with a Courant number of 0.5. This kind of solver has been already used in previous studies [4, 5, 11] providing precise and robust treatment of the Euler equations containing stiff chemical terms.
The ghost point technique is applied to manage the boundary conditions. It consists in adding three external rows of mesh points (half width of the WENO stencil) along the boundaries. Flow state at the external (ghost) points is determined according to the boundary type. For a periodic, symmetry and outflow boundaries, inner points are used to update ghost points at each time-step iteration. The injection boundary is treated as a symmetry plane, whereas injection fluxes are introduced as source terms in the lowermost row of internal points. Pressure at these points is taken as the wall pressure, P_w, to determine the injection sources as explained above.

3.4 Computational mesh adaptation and numerical resolution

Simulation of the CDWRE chamber operation is connected with specific issues. Whereas the compression and combustion processes within detonation waves are extremely rapid, the overall convective motion of the flow is

several orders of magnitude slower. As the detonation propagation simulation requires fine spatial and temporal resolution, resolution of the entire flowfield on a uniform mesh necessitates a very large number of mesh points and time steps. This represents an important difficulty especially for 3D simulations. It is evident that the flow zones that need to be finely resolved are around the detonation waves and the free surface of the fresh mixture layer. One can see from Fig. 1 that these zones represent a small fraction of the combustion chamber volume. Hence it is possible to reduce the computational cost by using local mesh refinement, which must be dynamically adapted to the flowfield evolution. In the present study the Adaptive Mesh Refinement (AMR) method is employed to manage the computational mesh.

According to the original method proposed by Berger and Collela [18], AMR consists in obtaining a numerical solution on block-structured meshes that constitute a mesh hierarchy. Starting from a base-level mesh, which is the coarsest one and covers the whole computational domain, the mesh hierarchy is composed of rectangular blocks of different levels so that higher level blocks are nested within lower level ones. Each refined level is characterized by a constant refinement factor, r, which represents the ratio of spatial steps of the parent mesh to the refined one in any of the mesh directions. For a refined mesh, the time step is proportionally reduced with respect to the parent mesh. Block boundaries are treated using the ghost point method by taking the solution from sibling or parent blocks to update the ghost points. More details on the AMR method can be found in [18, 19].

Among existing open-source implementations of AMR, AMROC [19] is the most suitable one for our purposes. AMROC is currently realized with different Euler solvers, based on TVD and WENO schemes, and integrated in the VTF software [20]. This is a sophisticated code that can be run on parallel computational platforms. For the present study, the WENO-based Euler solver, described above, has been implemented in the VTF framework. New FORTRAN modules for the numerical fluxes, time integration, thermodynamic and chemical kinetic models have been created by the authors.

Accurate resolution of the detonation wave structure requires that the spatial resolution of few micrometers under conditions considered in the present study. With this resolution, the mesh size is prohibitively large for our computational resources even if AMR is used. In the previous studies [4, 5], it was found that it was possible to obtain correct results on the detonation propagation velocity and overall variation of flow conditions across a detonation wave with a much coarser resolution. A 100 μm mesh step in x and y directions is fixed as necessary minimum for the particular conditions of the present study. For the z direction in 3D, a 100 μm resolution is too coarse to resolve the boundary of the fresh mixture jet; a 8.3 μm mesh step is used in this direction. The AMR refinement factor is $r = 3$ that corresponds the half-width of the WENO stencil. This choice allows minimizing the number of ghost points around the mesh blocks. One refinement level is used in 2D simulations and two levels in 3D.

4. Computational results

4.1 2D flowfield

An instantaneous flowfield, obtained from a 2D simulation, is shown in Fig. 3. The numerical Schlieren picture is represented by the field of density gradient magnitude in a normalized exponential scale. Superimposed streamlines are plotted in the moving reference frame attached to the detonation front.

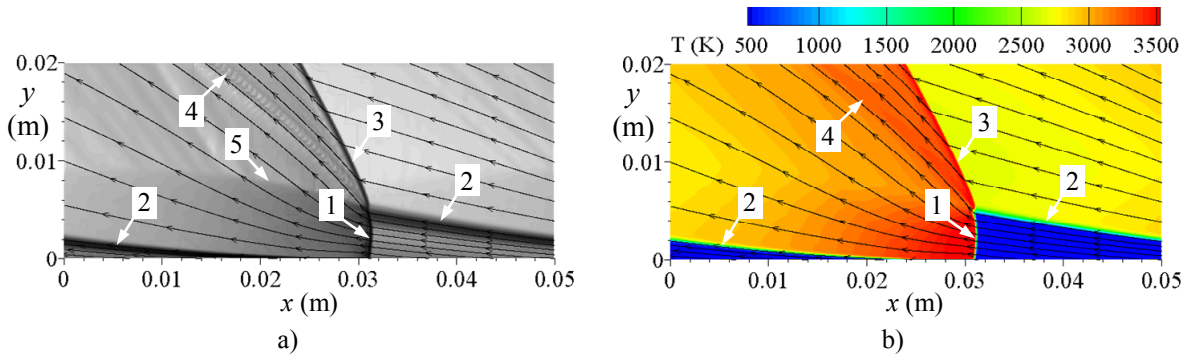

Figure 3: 2D instantaneous fields of density gradient (a) and static temperature (b) with streamlines in the moving reference frame: 1 – detonation wave; 2 – edge of the fresh mixture layer; 3 – oblique choc; 4 – slip line; 5 – boundary at the end of expansion fan

Main features of the flow structure can be easily distinguished. The detonation wave (1) is almost normal to the injection boundary and becomes oblique toward the edge of the mixture layer. The detonation results in a strong increase of pressure (by a factor of 20) and temperature (by a factor of 13). Combustion products expand behind the

detonation wave as indicated by the streamlines divergence. At a certain distance from the detonation wave, the wall pressure, P_w, is greater than the injection pressure, P_{tj}, hence the injection is blocked in that zone. From the point where $P_w = P_{tj}$, the layer of fresh mixture is continuously growing to $h \approx 4.5$ mm before the next detonation arrives. The mixture layer edge (2) is clearly marked in the temperature field. Interaction between the high-pressure flow generated by this detonation and already expanded flow from the previous one results in three waves: an expansion fan (5) centered at the top of the detonation front, an oblique shock (3) that recompresses the flow from previous detonation, and a slip line (4) that separates the two flows having different velocities and static temperatures. These three waves are originating from the point where the detonation front meets the edge of the fresh mixture layer.
The 2D case is convenient to illustrate how the computational mesh is managed by the AMR method. Figure 4 presents an instantaneous temperature field and corresponding snapshots of the refined mesh zone and the repartition of the computational domain between parallel processors. Black zone in Fig. 4a corresponds to the refined mesh. One can see that the refined mesh covers the regions of rapid variation of flow conditions whereas the most part of the flowfield is resolved on the base-level mesh. This simulation was run on 16 processors. The mesh hierarchy was updated every base-level time step. The domain repartition between parallel processors is also dynamically adapted providing necessary balancing of computational load. Zones of different colors in Fig. 4b correspond to different processes of parallel computation.

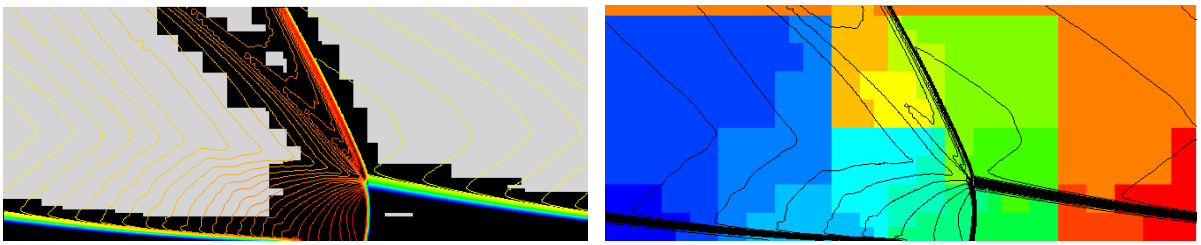

a) b)

Figure 4: Zone of refined mesh (a) and repartition of the computational domain between parallel processors (b) with superimposed isolines of an instantaneous temperature field

4.2 3D flowfield

An instantaneous flowfield, obtained from a 3D simulation, is shown in Fig. 5. The same kinds of flowfields as in 2D (see Fig. 3) are presented for the symmetry plane of the duct. The white dashed line corresponds to the injection slot edge. One can recognize the same features of the flowfield structure. On the other hand, the 3D flowfield is much more perturbed than the 2D one. The Schlieren picture shows intense turbulence, which perturbs the fresh mixture layer from the very beginning of its formation, and further, these perturbations affect the detonation, whose front is no more smooth as in 2D. The detonation front perturbations generate pressure fluctuations that are fed back to the flowfield and maintain the turbulence. In comparison with the 2D results, the mixture layer is almost twice higher.

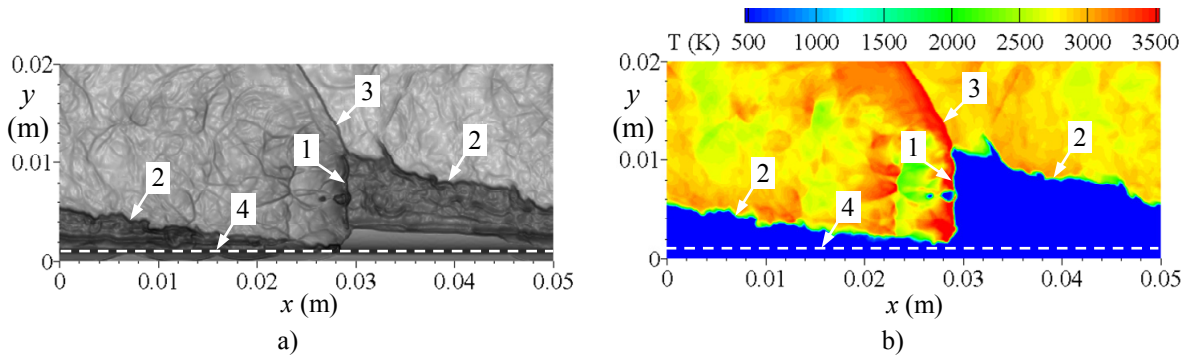

a) b)

Figure 5: Instantaneous fields of density gradient (a) and static temperature (b) in the symmetry plane of the 3D duct: 1 – detonation front; 2 – edge of the fresh mixture layer; 3 – oblique choc; 4 – injection slot edge

To illustrate the 3D flow, the instantaneous field of temperature is shown in Fig. 6. The symmetry plane is situated on the front side, whereas the dark background corresponds to the duct wall. From the 3D representation of temperature isosurfaces (Fig. 6a), one can notice that the flow turbulence is developed everywhere in the duct. The blue surface, which envelops the fresh mixture zone, has a marked wavy shape caused by flow fluctuations. Behind the detonation wave, the temperature field is very nonhomogeneous due to the fluctuating intensity of the detonation

front. In the *y*-*z* cuts of the temperature field, one can see how the fresh mixture jet develops in the duct. The mixture layer is localised in the middle of the duct and is quite narrow in comparison with the duct width. This explains why its height is much larger than in the 2D simulation. The jet boundary is very irregular and demonstrates important mixing between the fresh reactants and surrounding hot gases.

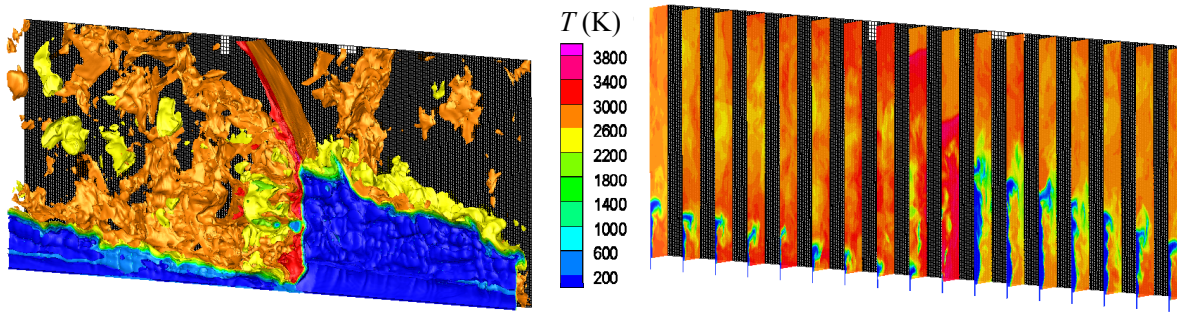

Figure 6: 3D field of static temperature: isosurfaces (a) and *y*-*z* cuts (b)

4.3 Analysis of detonation propagation conditions

The detonation propagation velocity is an important characteristic of CDWRE operation. The propagation velocity in the laboratory reference frame, u_D, characterizes the detonation frequency. The mean value of u_D obtained from the 2D simulation is 2775 m/s and the corresponding frequency is $f_D = u_D / l = 55.5$ kHz. It is also important to evaluate the detonation velocity with respect to the fresh mixture, D. The 2D simulation provided a mean value of D equal to 2814 m/s, which is close to the Chapman-Jouguet velocity $D_{CJ} = 2862$ m/s. D_{CJ} is evaluated for average static parameters of fresh mixture in front of the detonation.

Conditions of detonation propagation in 3D are analyzed for two instantaneous flowfields in the symmetry plane separated by a time interval of 8 μs. These time instants are designated as t1 and t2. For each time instant, profiles of static pressure and temperature along the *y*-axis are extracted at a short distance in front of the detonation. These profiles are defined as the pre-detonation state. The post-detonation state is obtained at the local pressure maximum for each horizontal row of mesh points. Finally, the Chapman-Jouguet (CJ) state is determined by thermodynamic computations for each point, representing the pre-detonation state. Profiles corresponding to these three states are plotted in Fig. 7. As one can see from these plots, the mixture does not detonate in the injection slot ($y < 0.9$ mm), hence the pressure and temperature do not change. Outside the slot ($y > 0.9$ mm), the flow parameter profiles are typical for an underexpanded jet: the fresh mixture flow quickly expands, then it is recompressed in a normal shock at $y \approx 3$ mm. After the normal shock, the flow parameters fluctuate near some constant level up to the top of the detonation front. By comparing the profiles corresponding to the post-detonation and CJ states, one can see that there exists a good general correspondence between these two states within the zone above the normal shock ($y > 3$ mm).

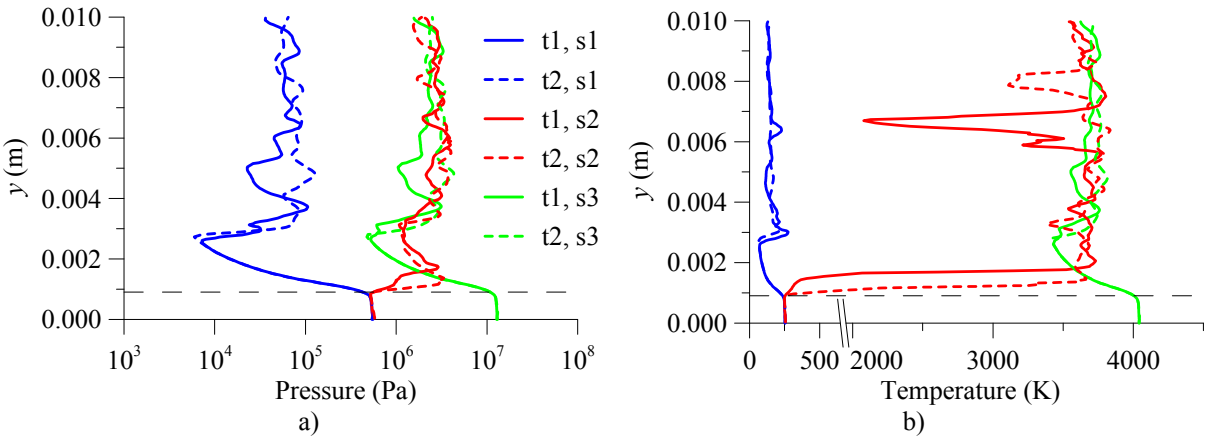

Figure 7: Profiles of pressure (a) and temperature (b) in the symmetry plane for time instants t1 and t2, and three gas states: s1 – pre-detonation; s2 – post-detonation; s3 – CJ

During a simulation, time instants corresponding to pressure spikes caused by the detonation were registered by several sensors forming an orthogonal grid in the symmetry plane: 5 vertical rows of 4 sensors in each row. Detonation front positions at different vertical distances are presented versus time in Fig. 8 together with a linear fit. The points, corresponding to the same x-coordinate, are almost coincident and lie close to the linear fit. This means that the detonation front preserves its vertical orientation during propagation. From the fit slope, the propagation velocity is 2880 m/s. Profiles of theoretical CJ velocity, calculated for t1 and t2, are traced in Fig. 9 in comparison with the propagation velocity obtained from the 3D simulation. One can note fairly good correspondence between the measured velocity and the CJ velocity above the normal shock ($y \geq 4$ mm). One can conclude from this analysis that, in case of slot injection, the detonation propagation is defined by the fresh mixture conditions in the jet past the normal shock. Prediction, based on the sonic flow conditions in the slot, results in an overestimation by about 2 %.

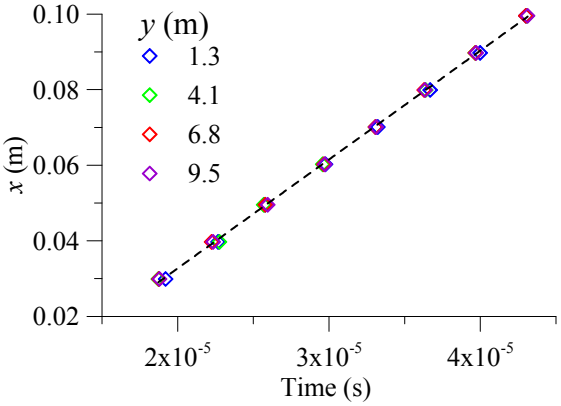

Figure 8: x-coordinate of the detonation wave versus time for different vertical positions of sensors

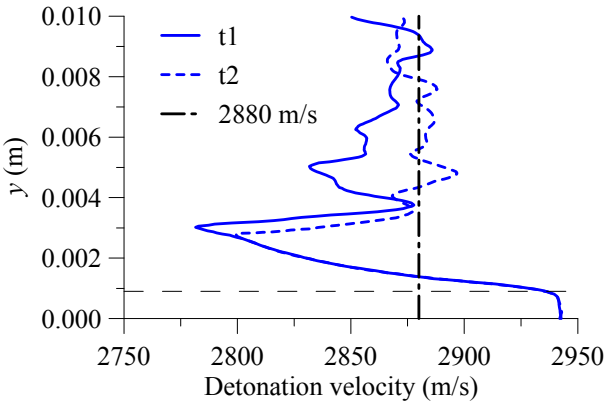

Figure 9: Profile of local CJ velocity evaluated for the pre-detonation conditions

5. Conclusion

A comparative analysis of 2D and 3D simulation results on a continuous detonation in stoichiometric H_2-O_2 mixture has been carried out. The principal difference between these configurations is related to the injection: in 2D, injection is uniformly distributed over the injection wall, whereas in 3D, the mixture is injected through a slot. Due to the slot injection, the height of the fresh mixture layer in front of the detonation is about twice larger, however in the z-direction, the fresh mixture fills a narrow zone in the middle of the duct. The 3D flowfield demonstrates an important level of turbulence that is due to hydrodynamic instabilities of the fresh mixture layer. In both cases, the detonation propagates in the Chapman-Jouguet mode, which is defined by the fresh mixture conditions in front of the detonation wave.

Acknowledgement

This work is financially supported by CNRS and MBDA France. The computational resources are provided by the Center of Scientific Computations of Région Centre (CCSC) and by the Computational Centre of IDRIS.

References

[1] Zhdan, S. A., Mardashev, A. M., and Mitrofanov, V. V. 1990. Calculation of the flow of spin detonation in an annular chamber. *Combustion Explosion and Shock Waves* 26:210-214.

[2] Zhdan, S. A., Bykovskii, F. A., and Vedernikov, E. F. 2007. Mathematical modeling of a rotating detonation wave in a hydrogen-oxygen mixture. *Combustion Explosion and Shock Waves*, 43:449-459.

[3] Hishida, M., Fujiwara, T., and Wolanski, P. 2009. Fundamentals of rotating detonations. *Shock Waves*, 19(1):1-10.

[4] Davidenko, D., Gökalp, I., and Kudryavtsev, A. 2008. Numerical study of the continuous detonation wave rocket engine. AIAA 2008-2680. *15th AIAA International Space Planes and Hypersonic Systems and Technologies Conference*.

[5] Davidenko, D. M., Gökalp, I., and Kudryavtsev, A. N. 2010. Numerical simulation of continuous detonation in a layer of hydrogen-oxygen mixture with periodic conditions. In: *Deflagrative and detonative combustion*, G. Roy and S. Frolov (eds.). Torus Press, Moscow. 407-422.
[6] Yamada, T., Hayashi, A. K., Yamada, E., Tsuboi, N., Tangirala, V. E., and Fujiwara, T. 2010. Detonation limit thresholds in H_2/O_2 rotating detonation engine. *Combustion Science and Technology*. 182(11):1901-1914.
[7] Shao, Y. T., Liu; M., and Wang, J. P. 2010. Numerical Investigation of Rotating Detonation Engine Propulsive Performance. *Combustion Science and Technology*. 182:1586–1597.
[8] Shao, Y. T., Liu; M., and Wang, J. P. 2010. Continuous detonation engine and effects of different types of nozzle on its propulsion performance. *Chinese Journal of Aeronautics*, 23:647-652.
[9] Yi, T. H., Turangan, C., Lou, J., et al. 2009. A three-dimensional numerical study of rotational detonation in an annular chamber. AIAA 2009-634. *47th Aerospace Sciences Meeting*.
[10] Yi, T. H., Lou, J., Turangan, C., et al. 2010. Effect of nozzle shapes on the performance of continuously rotating detonation engine. AIAA 2010-152. *48th AIAA Aerospace Sciences Meeting*.
[11] Eude, Y., Davidenko, D. M., Gökalp, I., and Falempin, F. 2011. Use of the adaptive mesh refinement for 3D simulations of a CDWRE (Continuous Detonation Wave Rocket Engine). AIAA 2011-2236. *17th AIAA International Space Planes and Hypersonic Systems and Technologies Conference*.
[12] Bykovskii, F. A., Zhdan, S. A., and Vedernikov, E. F. 2006. Continuous Spin detonations. *J. Propulsion and Power*. 22:1204-1216.
[13] Bykovskii, F. A., Zhdan, S. A., and Vedernikov, E. F. 2008. Continuous spin detonation of hydrogen-oxygen mixtures. 1. Annular cylindrical combustors. *Combustion Explosion and Shock Waves*. 44(2):150-162.
[14] Davidenko, D.M., Gökalp, I., Dufour, E., and Magre, P. 2006. Systematic numerical study of the supersonic combustion in an experimental combustion chamber. AIAA-2006-7913. *14th AIAA/AHI Space Planes and Hypersonic Systems and Technologies Conference*.
[15] Burcat, A. and Ruscic, B. 2005. Third millennium ideal gas and condensed phase thermochemical database for combustion with updates from active thermochemical tables. Argonne National Laboratory Report ANL-05/20. Technion Report TAE 960.
[16] Jiang, G.-S. and Shu, C.-W. 1996. Efficient implementation of weighted ENO schemes. *J. Comput. Phys.* 126:202-228.
[17] Zhong, X. 1996. Additive semi-implicit Runge-Kutta methods for computing high-speed nonequilibrium reactive flows. *J. Comput. Phys.* 128:19-31.
[18] Berger, M. J. and Colella, P. 1989. Local adaptive mesh refinement for shock hyprodynamics. *J. Comput. Phys.* 82:64-84.
[19] Deiterding, R. 2003. Parallel adaptive simulation of multi-dimensional detonation structures. Ph.D. thesis of Brandenburgischen Technischen Universität. Cottbus, Germany.
[20] The virtual test facility. California Institute of Technology.
URL: http://www.cacr.caltech.edu/asc/wiki/bin/view/Main/WebHome/